JACS
JOURNAL OF THE AMERICAN CHEMICAL SOCIETY
Article
pubs.acs.org/JACS

# Formation of S–Cl Phosphorothioate Adduct Radicals in dsDNA S-Oligomers: Hole Transfer to Guanine vs Disulfide Anion Radical Formation

Amitava Adhikary, Anil Kumar, Brian J. Palmer, Andrew D. Todd, and Michael D. Sevilla*

Department of Chemistry, Oakland University, Rochester, Michigan 48309, United States

Supporting Information

**ABSTRACT:** In phosphorothioate-containing dsDNA oligomers (S-oligomers), one of the two nonbridging oxygen atoms in the phosphate moiety of the sugar–phosphate backbone is replaced by sulfur. In this work, electron spin resonance (ESR) studies of one-electron oxidation of several S-oligomers by $Cl_2^{\bullet-}$ at low temperatures are performed. Electrophilic addition of $Cl_2^{\bullet-}$ to phosphorothioate with elimination of $Cl^-$ leads to the formation of a two-center three-electron $\sigma^2\sigma^{*1}$-bonded adduct radical (-P-S∴Cl). In AT S-oligomers with multiple phosphorothioates, i.e., d[ATATAsTsAsT]$_2$, -P-S∴Cl reacts with a neighboring phosphorothioate to form the $\sigma^2\sigma^{*1}$-bonded disulfide anion radical ([-P-S∴S-P-]$^-$). With AT S-oligomers with a single phosphorothioate, i.e., d[ATTTAsAAT]$_2$, reduced levels of conversion of -P-S∴Cl to [-P-S∴S-P-]$^-$ are found. For guanine-containing S-oligomers containing one phosphorothioate, -P-S∴Cl results in one-electron oxidation of guanine base but not of A, C, or T, thereby leading to selective hole transfer to G. The redox potential of -P-S∴Cl is thus higher than that of G but is lower than those of A, C, and T. Spectral assignments to -P-S∴Cl and [-P-S∴S-P-]$^-$ are based on reaction of $Cl_2^{\bullet-}$ with the model compound diisopropyl phosphorothioate. The results found for d[TGCGsCsGCGCA]$_2$ suggest that [-P-S∴S-P-]$^-$ undergoes electron transfer to the one-electron-oxidized G, healing the base but producing a cyclic disulfide-bonded backbone with a substantial bond strength (50 kcal/mol). Formation of -P-S∴Cl and its conversion to [-P-S∴S-P-]$^-$ are found to be unaffected by $O_2$, and this is supported by the theoretically calculated electron affinities and reduction potentials of [-P-S-S-P-] and $O_2$.

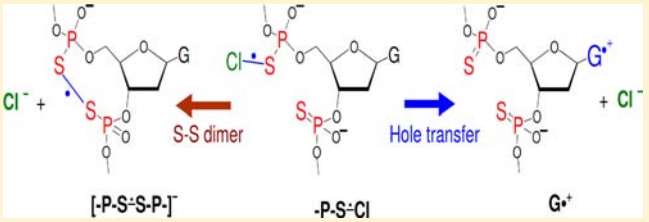


## 1. INTRODUCTION

Ionizing radiation is known to induce frank DNA-strand breaks—particularly, of double-strand breaks that are associated with cell death, mutation, aging, and transformation.[1−4] One-electron oxidation of the sugar–phosphate backbone creates an electron loss center (hole) which upon deprotonation forms a sugar radical, and these are the immediate precursors of radiation-induced frank DNA-strand breaks produced via the electron-loss (oxidative) pathway.[1,4−13] Hole transfer from the sugar–phosphate backbone to a DNA base creates a base cation radical which prevents formation of sugar radicals via deprotonation (Scheme 1).[5−7,11,12,14−19] Our recent work[14] has shown that, for successful formation of a sugar radical (for example, C5′$^\bullet$), a very rapid ($<10^{-12}$ s) deprotonation must occur from the one-electron-oxidized sugar–phosphate backbone before a competitive backbone-to-base hole transfer can occur (Scheme 1). This work has also shown that in both ion-beam and $\gamma$-irradiated DNA, C5′$^\bullet$ is formed by fast deprotonation at 77 K, even though longer-lived holes and electrons trapped on DNA bases are successfully scavenged at 77 K.[14] Measurement of unaltered base release is considered a monitor of sugar radical formation from irradiated DNA.[4−7] Yields of unaltered base release in DNA pellets $\gamma$-irradiated at 77 K, have suggested that considerable backbone-to-base hole transfer occurs after ionization of the sugar–phosphate DNA backbone[20−22] with a majority of the holes from the ionized sugar–phosphate backbone transferring to the bases at 77 K. Thus, the rate and extent of hole transfer from the sugar–phosphate backbone to the base is critically controlled by fast proton-transfer processes from the nascent electron-deficient radical (Scheme 1).[14] If the lifetime of the hole in the sugar–phosphate backbone could be increased, electron spin resonance (ESR) spectroscopy could be employed to study directly the processes involved in backbone-to-base hole transfer (Scheme 1).

S-Oligomers are being actively pursued as antisense DNA-oligomers to regulate gene expression.[23−25] Recent work has established that the phosphorothioate modification observed in an S-oligomer is a naturally occurring product of dnd genes found in bacteria and archea.[26] Substitution of one of the oxygen atoms in the phosphate moiety of DNA backbone by sulfur (i.e., phosphorothioate) causes minimum perturbation of DNA base stacking and DNA conformation.[27,28] In S-oligomers, the negative charge on the phosphate moiety is retained and owing to the substitution of one of phosphate oxygen atoms by a sulfur atom it can be expected that the ionization potential as well as the one-electron oxidation

Received: June 18, 2013
Published: July 25, 2013



dx.doi.org/10.1021/ja406121x | J. Am. Chem. Soc. 2013, 135, 12827−12838

**Scheme 1. Competition between Backbone-to-Base Hole Transfer (ht) and Sugar Radical Formation (e.g., C5′•) via Deprotonation of the One-Electron-Oxidized Sugar−Phosphate**

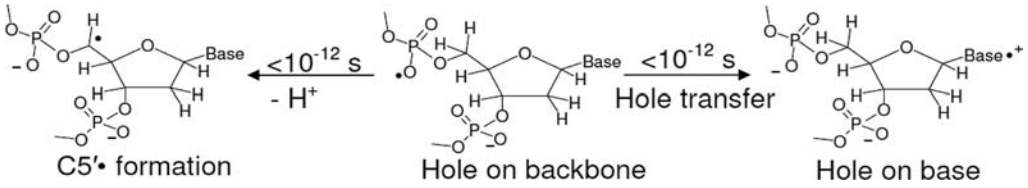


potential of the phosphorothioate moiety in the S-oligomer should be lower than those for the phosphate moiety in the unmodified oligomer. As a result, the holes formed either via ionization or via one-electron oxidation of the phosphorothioate moiety in the S-oligomers could be more stabilized allowing time to investigate backbone-to-base hole transfer. In this work, ESR spectroscopic studies have been carried out on S-oligomers to look for one-electron oxidation of the phosphorothioate backbone by $Cl_2^{\bullet-}$ and possible backbone-to-base hole transfer.

Employing diisopropyl phosphorothioate as a model compound of phosphorothioate and S-oligomers of GC and AT sequences and $Cl_2^{\bullet-}$ as one-electron oxidant in the glassy system (7.5 M LiCl in $D_2O$ at low temperatures), we find evidence regarding formation of the three-electron bonded adduct radical (-P-S∴Cl), which is presented in this work. This work shows that, upon temperature-dependent progressive annealing, the -P-S∴Cl results in one-electron oxidation of G but not A, C, or T. Thus, the one-electron redox potential of -P-S∴Cl is bracketed between those of G and A. Moreover, the -P-S∴Cl radical also reacts with a second phosphorothioate to form the dimer disulfide anion radical $[\text{-P-S}^{\therefore}\text{S-P-}]^-$ in model systems and in DNA oligomers. The number as well as the proximity of phosphorothioate moieties dictate the nature (unimolecular or bimolecular) formation of $[\text{-P-S}^{\therefore}\text{S-P-}]^-$. In S-oligomers having GC sequences with two phosphorothioate moieties in close proximity, ESR studies have provided the evidence of electron transfer from $[\text{-P-S}^{\therefore}\text{S-P-}]^-$ to one-electron-oxidized guanine. Radical identities are confirmed by density functional theory (DFT) calculations of hyperfine coupling constants of both -P-S∴Cl and $[\text{-P-S}^{\therefore}\text{S-P-}]^-$ in the model compound and in S-oligomers. Experiment and theory provide for the prediction of electron affinities and one-electron redox potentials of -P-S∴Cl and [-P-S-S-P-]. Theoretical calculations have been carried out to estimate the adiabatic ionization energies of dimethyl phosphorothioate and dimethylphosphate as well as the bond dissociation energy of the two-center three-electron $\sigma^2\sigma^{*1}$-bonded -P-S∴Cl and $[\text{-P-S}^{\therefore}\text{S-P-}]^-$ systems.

## 2. MATERIALS AND METHODS

**2.1. Compounds.** The phosphorothioate model compound diisopropyl phosphorothioate (DIP) and lithium chloride (99% anhydrous, Sigma Ultra) were procured from Sigma Chemical Co. (St. Louis, MO). Potassium persulfate (crystal) was obtained from Mallinckrodt, Inc. (Paris, KY). Deuterium oxide (99.9 atom % D) was obtained from Aldrich Chemical Co. Inc. (Milwaukee, WI).

Double-stranded (ds) DNA S-oligomers such as d-$[TGCGsCGCGCA]_2$, d$[TGCGsCsGCGCA]_2$, d$[ATTTAsAAT]_2$, d-$[ATTTAsAsAsT]_2$, and d$[ATATAsTsAsT]_2$ were obtained from SynGen, Inc. (Hayward, CA). In all these sequences, the symbol "s" denotes substitution of phosphate by phosphorothioate moiety. These S-oligomers were lyophilized, desalted, and column-purified. The modified column purification protocol with extended wash steps was applied by SynGen, Inc. to ensure the complete removal of reported organic contaminants such as "benzoyl" [29] from these ds S-oligomers.

All compounds were used without any further purification.

**2.2. Preparation of Solutions.** *2.2.1. DIP Solution Preparations.* Following our previous works with the monomeric model compounds of DNA and RNA,[5−7,14,17,18,30−43] homogeneous solutions of DIP have been prepared by dissolving ∼2 mg of DIP in 1 mL of 7.5 M LiCl in $D_2O$ (pH ∼5) in the presence of 6 mg of $K_2S_2O_8$ as the electron scavenger.

*2.2.2. dsDNA S-Oligomer Solution Preparations.* As per our continuing efforts using DNA and RNA oligomers,[5−7,14,17,18,30−43] homogeneous solutions of these S-oligomers are prepared by dissolving 1.1−1.6 mg of a S-oligomer in 1 mL of 7.5 M LiCl/$D_2O$ with occasional vortexing. Thereafter, 8−10 mg is $K_2S_2O_8$ is added as the electron scavenger.

We have already shown that the dsDNA 8-mer d$[TGCGCGCA]_2$ remains double-stranded in 7.5 M LiCl in $D_2O$ up to 48 °C.[42] The dsDNA oligomers in homogeneous aqueous ($H_2O$) glasses (10 M LiCl) have been reported to be in the B-conformation.[44] It has already been mentioned (see Introduction) that the crystal structures of unmodified and phosphorothioate-modified dsDNA-oligomers have been found to be very similar.[27,28] Thus, it can be concluded that in our system (homogeneous solutions of an S-oligomer in 7.5 M LiCl in $D_2O$), S-oligomers are double-stranded.

Employing $K_2S_2O_8$ as the electron scavenger, only the formation of one-electron-oxidized radicals and their reactions are studied in our system.

**2.3. Preparation of Glassy Samples and Their Storage.** Homogenous solutions of DIP were thoroughly bubbled with nitrogen to remove oxygen. For oxygen reaction studies, matched DIP solutions were saturated with oxygen. The homogeneous solutions of ds S-oligomers were thoroughly bubbled with nitrogen to remove oxygen. Thereafter, as per our previous efforts,[5−7,14,17,18,30−43] these homogeneous solutions of DIP and the dsDNA S-oligomers are drawn into 4 mm Suprasil quartz tubes (catalog no. 734-PQ-8, WILMAD Glass Co., Inc., Buena, NJ). Subsequently, these tubes containing these solutions are rapidly cooled to 77 K. This rapid cooling of these liquid solutions results into the transparent glassy solutions which are later used for the irradiation and subsequent progressive annealing experiments. All samples are stored at 77 K in Teflon containers in the dark.

**2.4. $\gamma$ Irradiation of Glassy Samples and Their Storage.** Following our works,[37,45] the glassy samples in Teflon containers were placed in a 400 mL styrofoam dewar under liquid nitrogen (77 K). The styrofoam dewar was then placed into the 109-GR 9 irradiator that contains a properly shielded $^{60}$Co gamma source so that the $\gamma$ irradiation of the glassy samples were performed at 77 K to an absorbed dose of 1.4 kGy. These $\gamma$-irradiated samples are stored at 77 K in the dark in Teflon containers for ESR analyses.

**2.5. Annealing of the Samples.** As per our work with dsDNA-oligomers,[42,43] annealing ESR studies of these $\gamma$-irradiated glassy samples are carried out in the range 155−175 K.

Employing a variable temperature assembly (Air products) via cooled nitrogen gas in the dark which regulated the gas temperature within 4 K, annealing studies for these samples are carried out.

The annealing of the sample softens the glass thereby allowing matrix radicals, e.g., $Cl_2^{\bullet-}$ to migrate and react with solute (either DIP or ds S-oligomer). Formation of sulfur-centered adduct radical (-P-S∴Cl) in DIP and S-oligomers are produced by reaction with


dx.doi.org/10.1021/ja406121x | J. Am. Chem. Soc. 2013, 135, 12827−12838

$Cl_2^{\bullet-}$ on annealing in the temperature range 100−160 K (see Results). Subsequent reactions of -P-S∴Cl are followed by ESR spectroscopy upon further annealing these samples in the temperature range 155−180 K, for 15−20 min (see Results). After annealing, these samples were immersed in liquid nitrogen (77 K) and stored.

**2.6. Electron Spin Resonance.** Following $\gamma$-irradiation and annealing, these glassy samples are immersed immediately in liquid nitrogen and ESR spectra are recorded at 77 K and at 40 dB (20 $\mu$W) power as well as 30 dB (0.2 mW) for the -P-S∴Cl radical which is less prone to power saturation than other DNA radicals. Fremy's salt (with $g$(center) = 2.0056, $A_N$ = 13.09 G) has been used for field calibration.[22,37,45] We have recorded these ESR spectra using a Varian Century Series ESR spectrometer operating at 9.3 GHz with an E-4531 dual cavity, 9-in. magnet and with a 200 mW klystron.[22,37,45] Following our works,[30,37] the simulated spectra are obtained to fit the experimentally recorded spectra employing anisotropic simulations. These simulations have been carried out by WIN-EPR and SimFonia (Bruker) programs. All the ESR spectra reported in this work have been recorded at 77 K.

**2.7. Calculations Based on Density Functional Theory.** Becke's three-parameter exchange functionals (B3)[46,47] with Lee, Yang, and Parr's correlation functional (LYP)[48] and 6-31G* basis set has been designated as the B3LYP/6-31G* method. Our works[5−7,14,17,18,30−43] along with the works of others[49−52] have shown that the B3LYP method with the compact basis set 6-31G* is quite appropriate to obtain reliable hyperfine coupling constant (HFCC) values for radicals that are comparable to experimentally determined HFCCs. Therefore, the B3LYP/6-31G* method has been used in this work to study the optimized geometries, spin density and charge distributions, and the HFCC values of -P-S∴Cl and [-P-S∴S-P-]$^-$ in DIP (reactions 4 and 5) in the gas phase. The geometry of the

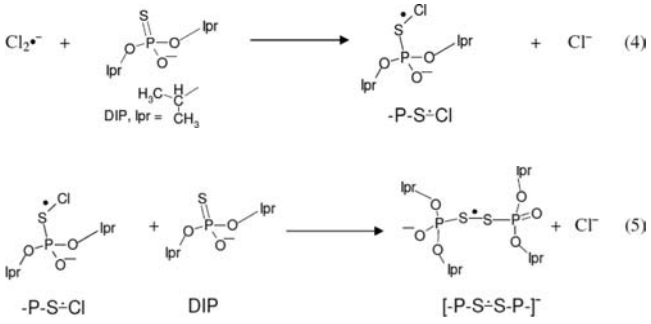


adenine dinucleoside diphosphorothioate, AsAs, has been fully optimized employing the M06-2x/6-31G** method because B3LYP is not suitable for stacked systems.[53] Spin density distributions along with the HFCC values of [-P-S∴S-P-]$^-$ in AsAs are calculated at the B3LYP/6-31G* level of theory in the gas phase. The 6-31++G(d) basis set was used to calculate the reduction potentials, adiabatic electron affinity (AEA), bond dissociation energy (BDE), and the adiabatic ionization energies (see section 3.2). All calculations reported in this work have been performed using Gaussian 09 suite of programs.[54] GaussView[55] and IQMOL[56] programs have been used to plot the spin densities, molecular orbitals, and molecular structures.

## 3. RESULTS AND DISCUSSION

**3.1. Experimental Results.** *3.1.1. Diisopropyl Phosphorothioate (DIP): The Model Compound. Formation of -P-S∴Cl Followed by Formation of Disulfide Anion Radical ([-P-S∴S-P-]$^-$) in DIP.* The ESR spectrum (black) of a $\gamma$-irradiated glassy (7.5 M LiCl/$D_2O$) sample of DIP (2 mg/mL) is shown in Figure 1A. When this spectrum (400 G scan) is compared with the central part of the total 880 G wide multiplet $Cl_2^{\bullet-}$ spectrum,[37,43] it is observed that the black spectrum contains only the expected two low field resonances from $Cl_2^{\bullet-}$ and a sharp singlet due to $SO_4^{\bullet-}$. Formation of

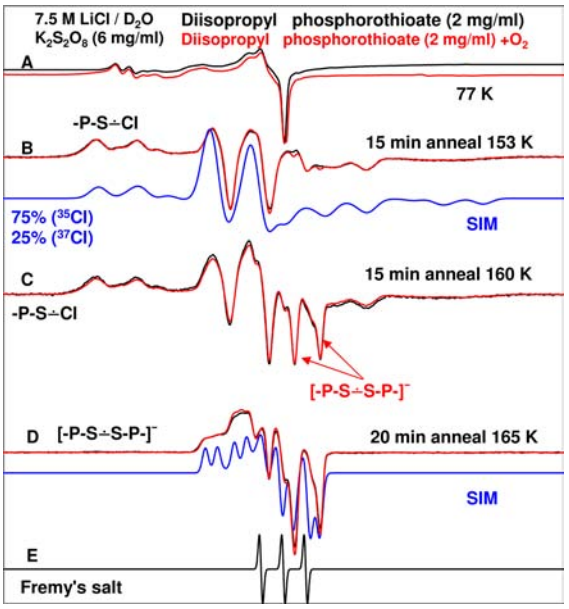


**Figure 1.** ESR spectra (black) of (A) $\gamma$-irradiated glassy sample of DIP (2 mg/mL in 7.5 M LiCl/$D_2O$) in the presence of electron scavenger $K_2S_2O_8$ (6 mg/mL) at pH ∼5. (B−D) Spectra found after annealing to (B) 153 K for 15 min, (C) 160 K for 15 min, (D) 165 K for 20 min. The blue spectra in (B) and (D) are the simulated spectra of -P-S∴Cl and [-P-S∴S-P-]$^-$, respectively. See text for details of simulation. The spectra in red are of a matched sample of DIP (2 mg/mL) in which oxygen was bubbled for 30 s are superimposed on the corresponding black spectra in (A)−(D) for comparison (all other conditions the same as black). (E) shows the position of three Fremy's salt resonances with the central one at $g$ = 2.0056. Each of these lines is separated from another by 13.09 G.

$Cl_2^{\bullet-}$ results from radiation-produced holes (reaction 1), whereas, the reaction of radiation-produced electrons with $S_2O_8^{2-}$ leads to the formation of $SO_4^{\bullet-}$ (reaction 2).[2−5] Formation of additional $Cl_2^{\bullet-}$ occurs on the reaction of $SO_4^{\bullet-}$ with $Cl^-$ upon annealing to 140 K (data not shown) as per our previous work (reaction 3).[5−7,31,57]

$$h^+ + 2Cl^- \rightarrow Cl_2^{\bullet-} \quad (1)$$

$$e^- + S_2O_8^{2-} \rightarrow SO_4^{2-} + SO_4^{\bullet-} \quad (2)$$

$$SO_4^{\bullet-} + 2Cl^- \rightarrow SO_4^{2-} + Cl_2^{\bullet-} \quad (3)$$

Annealing of this sample at 153 K for 15 min allows for the migration of the only remaining reactant species, $Cl_2^{\bullet-}$, which reacts with the solute (DIP), producing the black spectrum in Figure 1B, showing formation of a chlorine atom adduct radical species (-P-S∴Cl) whose three-electron bonding is $\sigma^2\sigma^{*1}$ in nature. This spectrum has a characteristic quartet owing to a single anisotropic Cl atom with an $A_{||}(^{35}Cl)$ of ∼67 G along with the central doublet due to an isotropic $\alpha$ P atom coupling of ∼23 G (see Table 2, below). An anisotropic simulation of this spectrum has been carried out. The simulated spectrum (blue) is an overlap of the spectra from two Cl isotopes ($A_{||}(^{35}Cl,75\%)$ = 67 G and $A_{||}(^{37}Cl,25\%)$ = 56 G, and $A_{\perp}$ = 0) along with a mixed Lorentzian/Gaussian (1/1) isotropic line width of 10 G and $g_{||}$ = 2.0028 and $g_{\perp}$ = 2.0014. The simulated spectrum (blue) matches the black spectrum quite well and supports our assignment of this black spectrum to -P-S∴Cl. Formation of this $\sigma^2\sigma^{*1}$-bonded adduct radical -P-S∴Cl occurs as shown in reaction 4.


dx.doi.org/10.1021/ja406121x | J. Am. Chem. Soc. 2013, 135, 12827−12838

The experimentally recorded spectrum (black) upon further annealing of this sample to 160 K is shown in Figure 1C. Comparison of spectrum 1C with spectrum 1B shows that the line components due to -P-S:Cl are still present while new line components assigned to the disulfide anion radical ([-P-S:S-P-]$^-$) (vide infra) produced via bimolecular reaction of -P-S:Cl with an unreacted DIP molecule (reaction 5):

The experimentally recorded spectrum (black) found on annealing to 165 K shown in Figure 1D is assigned to [-P-S:S-P-]$^-$. The spectrum shows two anisotropic couplings assigned to two $\alpha$ P atoms. A simulation of this spectrum employing two anisotropic $\alpha$ P atom couplings of (16.0, 16.0, 17.0) G and (6.0, 9.0, 7.0) G (see Table 2, below) along with a mixed Lorentzian/Gaussian (1/1) anisotropic line width (3.5, 4.5, 3.5) G and $g$-values (1.99939, 2.0046, 2.0270) shows a good match between the simulated (blue) and experimentally obtained (black) spectra.

Previous ESR work[58] with methionine, methionine peptides, and model compounds has shown the reaction of $Cl_2^{\bullet-}$ can also lead to formation of Cl−S adduct radical formation (-S:Cl). In this previous work,[58] -S:Cl adducts reacted with methionine to form disulfide cation radicals ([-S:S-]$^+$). In the current work, evidence of formation of the anion radical, [-P-S:S-P-]$^-$ via reaction 5 is presented. The assignment of [-P-S:S-P-]$^-$ is justified by theoretical calculations (see section 3.2). While methionine resulted in the disulfide cation radical and the phosphorothioate resulted in the disulfide anion radical both are the products of one-electron oxidation and subsequent reaction with the parent compound.

The spectra (red) of a matched sample of DIP (2 mg/mL) in which oxygen was bubbled for 30 s are superimposed on the corresponding black spectra for comparison. The virtually identical nature of the black and red spectra show that oxygen had no effect on the formation of the adduct radical -P-S:Cl or of [-P-S:S-P-]$^-$. Thus, contrary to various disulfide anion radical [R-S:S-R]$^-$,[59] Figure 1 shows that [-P-S:S-P-]$^-$ does not transfer an electron to oxygen (reaction 6), and thus, no observable decrease of ESR signal intensity of [-P-S:S-P-]$^-$ is observed resulting from the formation of neutral and diamagnetic [-P-S-S-P-].

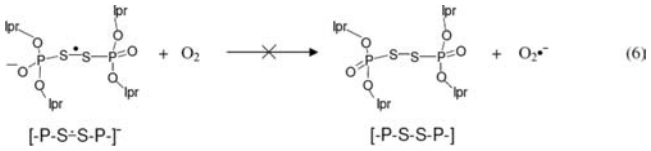


(6)

This result is in keeping with the theoretically calculated electron affinity value of [-P-S:S-P-]$^-$, which is found to be higher than that of molecular oxygen (see section 3.2). Thus, one-electron reduction of dioxygen by [-P-S:S-P-]$^-$ is not expected.

*3.1.2. S-Oligomers.* In this part of our experimental investigations of phosphorothioates, the reaction of $Cl_2^{\bullet-}$ with S-oligomers has been investigated. Here we investigate two competitive reactions: (a) one-electron oxidation of DNA bases by $Cl_2^{\bullet-}$ and (b) electrophilic addition of $Cl_2^{\bullet-}$ to the S atom of the phosphorothioate moiety followed by elimination of $Cl^-$ to form -P-S:Cl (reaction 4 and Scheme 2).

We find that, once formed, -P-S:Cl in an S-oligomer can undergo several competitive reactions. -P-S:Cl can result in one-electron oxidation of the DNA base moiety (backbone-to-base hole transfer, Schemes 1 and 2). Formation of [-P-S:S-P-]$^-$ can take place via reaction of -P-S:Cl with an unreacted phosphorothioate moiety (reaction 5) in the same strand or in the opposite strand of the same S-oligomer molecule. Intermolecular formation of [-P-S:S-P-]$^-$ can also occur via reaction of -P-S:Cl formed in an S-oligomer molecule with an unreacted phosphorothioate moiety of a second S-oligomer (Scheme 3). The rate and extent of these reactions depend on the number and proximity of the phosphorothioate backbone moieties.

We have investigated these reactions in S-oligomers composed of only AT (d[ATTTAsAAT]$_2$, d[ATATAsTsAsT]$_2$, d[ATATAsAsAsT]$_2$) (section 3.1.2.1) and S-oligomers composed of predominantly GC (d[TGCGsCGCGCA]$_2$, d-[TGCGsCsGCGCA]$_2$) (section 3.1.2.2). These results are described below.

*3.1.2.1. AT ds S-Oligomers with Consecutive Phosphorothioates.* Results obtained employing d[ATATAsTsAsT]$_2$ are found to be similar to those from d[ATATAsAsAsT]$_2$ (shown in Supporting Information Figure S1). Spectra of -P-S:Cl and [-P-S:S-P-]$^-$ are found to be similar in these S-oligomers, though d[ATATAsAsAsT]$_2$ has an AT mismatch. Hence, only the results of d[ATATAsTsAsT]$_2$ are shown in Figure 2.

In Figure 2A, the ESR spectrum of a $\gamma$-irradiated glassy sample of d[ATATAsTsAsT]$_2$ is presented. As found for the spectrum in Figure 1A, this spectrum contains only the low-field resonances from $Cl_2^{\bullet-}$ and a sharp component at $g$ = 2 from $SO_4^{\bullet-}$. On annealing to 140 K, the $SO_4^{\bullet-}$ reacts with $Cl^-$ to form additional $Cl_2^{\bullet-}$, and $Cl_2^{\bullet-}$ is the only species that reacts with the solute in this system.

Further annealing of this sample resulted in the spectra shown in Figure 2B at 160 K, Figure 2C at 165 K, and Figure 2D at 170 K. Using the black spectrum in Figure 1B as the benchmark spectrum for -P-S:Cl and the black spectrum in Figure 2E as the benchmark for [-P-S:S-P-]$^-$ in a ds S-oligomer (vide infra), analyses of these spectra show that they result from two radicals, viz. -P-S-Cl formed early and [-P-S:S-P-]$^-$ produced on prolonged annealing. Spectral analyses show that, on annealing, -P-S:Cl decreased from ∼70% at 160 K to ∼35% at 180 K along with the concomitant increase of [-P-S:S-P-]$^-$ from ∼30% at 160 K to ∼65% at 180 K. While the total signal decreased, the absolute intensity of [-P-S:S-P-]$^-$ has increased, and this is easily seen for the high-field component of [-P-S:S-P-]$^-$, which is marked with the red dotted line. These results provide evidence that -P-S:Cl results in the formation of [-P-S:S-P-]$^-$ (Scheme 3 and reaction 5) but does not cause one-electron oxidation of either A or T.

Subtraction (∼35%) of the spectrum in Figure 2C from spectrum 2D results in spectrum 2E, which has been assigned to [-P-S:S-P-]$^-$ in a ds S-oligomer. This spectrum shows two $\alpha$ P atom anisotropic couplings, one large and one small. A simulation of this spectrum employing two anisotropic $\alpha$ P atom couplings of (14.0, 16.0, 14.0) G and (2.0, 4.0, 4.0) G (see Table 2, below) along with a mixed Lorentzian/Gaussian (1/1) isotropic 3.0 G line width and $g$-values (1.9965, 2.0079, 2.0303) shows a good match between the simulated (blue) and experimentally obtained (black) spectra.

*3.1.2.2. AT S-Oligomers with One Phosphorothioate.* Here we investigate the extent of interstand and/or biomolecular formation of [-P-S:S-P-]$^-$ from -P-S:Cl for the case of a ds S-oligomer with a single phosphorothioate, d[ATTTAsAAT]$_2$.

Figure 3A shows the ESR results found for a matched sample of d[ATTTAsAAT]$_2$ that was $\gamma$-irradiated at 77 K and subsequently annealed to 160 K for 15 min. The spectrum in


dx.doi.org/10.1021/ja406121x | J. Am. Chem. Soc. 2013, 135, 12827−12838

**Scheme 2. Competitive Reactions of $Cl_2^{\bullet-}$ with an S-Oligomer To Form Base Cation Radical via Backbone-to-Base Hole Transfer or To Produce -P-S∴Cl**

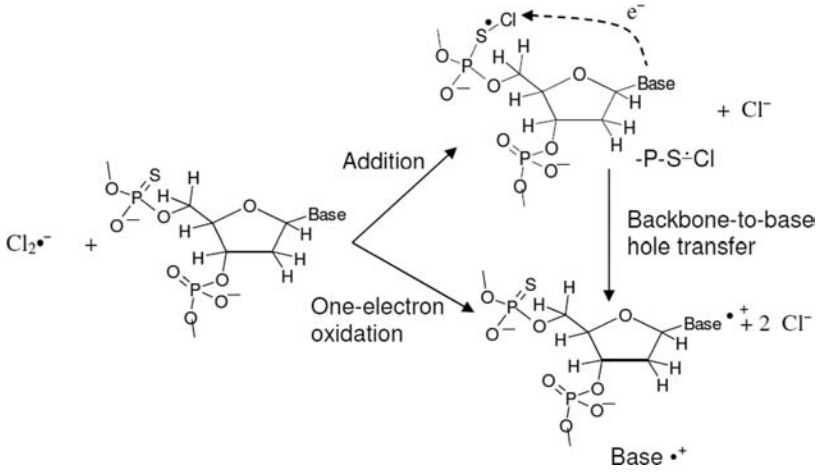


**Scheme 3. Competitive Reactions of -P-S∴Cl in a ds S-Oligomer**

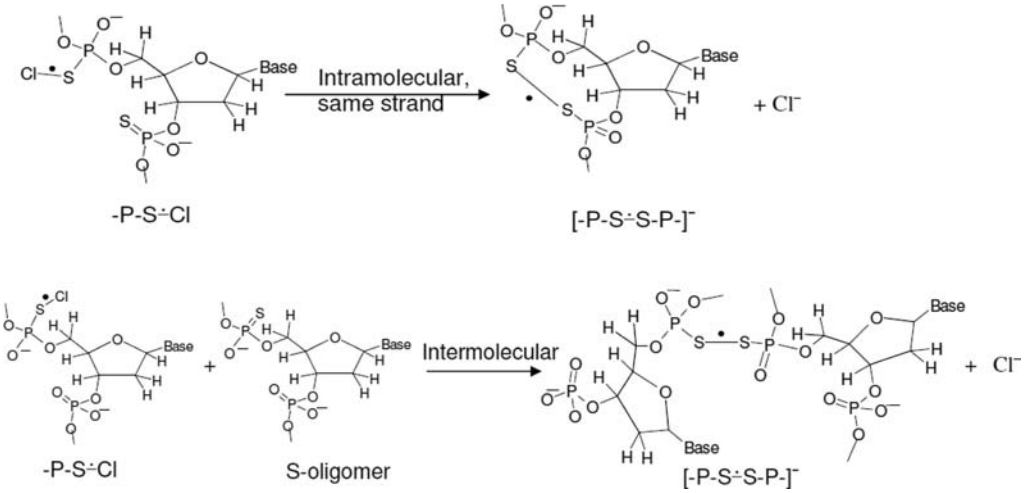


Figure 3B is obtained upon further annealing of this sample to 175 K. Spectra 3A and 3B are also found to result from two radicals, viz. -P-S∴Cl and $[\text{-P-S}^{\therefore}\text{S-P-}]^-$.

Using the same benchmark spectra as used in the analyses of the spectra in Figure 2 (vide supra), the extent of -P-S∴Cl conversion to $[\text{-P-S}^{\therefore}\text{S-P-}]^-$ (~35%) found on annealing is far less than that found for the S-oligomer with adjacent phosphorothioates in Figure 2 (65%).

Comparison of results found in Figures 1−3 leads to the following salient findings:

(i) The rate and extent of conversion of -P-S∴Cl to $[\text{-P-S}^{\therefore}\text{S-P-}]^-$ decreases considerably in ds S-oligomers compared to the monomeric model compound, DIP. In DIP, this conversion is complete at 165 K in our glassy system, while in ds S-oligomers, complete conversion of -P-S∴Cl to $[\text{-P-S}^{\therefore}\text{S-P-}]^-$ is not observed even upon annealing to 180 K. The decrease in the kinetics of conversion of -P-S∴Cl to $[\text{-P-S}^{\therefore}\text{S-P-}]^-$ from DIP to ds S-oligomers is attributed to steric factors associated with DNA structure which hinder dimerization.

(ii) The nature and extent of conversion of -P-S∴Cl to $[\text{-P-S}^{\therefore}\text{S-P-}]^-$ are critically dependent on the number and proximity of phosphorothioate moieties in the S-oligomer. The far lower conversion of -P-S∴Cl to $[\text{-P-S}^{\therefore}\text{S-P-}]^-$ in $d[ATTTAsAAT]_2$ than that in $d[ATATAsTsAsT]_2$ under identical conditions indicates that the formation of $[\text{-P-S}^{\therefore}\text{S-P}]^-$ shows a preference for reaction between near-neighbor phosphorothioates over between phosphorothiotes on opposite DNA strands in the same dsDNA molecule or intermolecularly between separate dsDNA molecules (Scheme 3).

(iii) Absence of formation of adenine and thymine cation radicals or their deprotonated forms shows that -P-S∴Cl cannot one-electron oxidize A and T, and hence no backbone-to-base hole transfer (Scheme 2) is possible in S-oligomers with A and T.

(iv) ESR line components resulting from sugar radical(s) were notobserved on annealing in S-oligomers.

(v) The mismatch in the S-oligomer $d[ATATAsAsAsT]_2$ did not affect formation of $[\text{-P-S}^{\therefore}\text{S-P-}]^-$ from -P-S∴Cl.

*3.1.2.3. ds S-Oligomers Containing Predominantly G and C: Backbone-to-Base Hole Transfer.* ESR investigations were carried out employing $d[TGCGsCGCGCA]_2$ to test for hole transfer from P-S∴Cl to G as well as $[\text{-P-S}^{\therefore}\text{S-P-}]^-$ formation (Schemes 2 and 3). These results are shown in Figure 4.

The ESR spectrum obtained using a sample of $d[TGCGsCGCGCA]_2$ that was γ-irradiated at 77 K and subsequently annealed to 160 K for 15 min is presented in


dx.doi.org/10.1021/ja406121x | J. Am. Chem. Soc. 2013, 135, 12827−12838

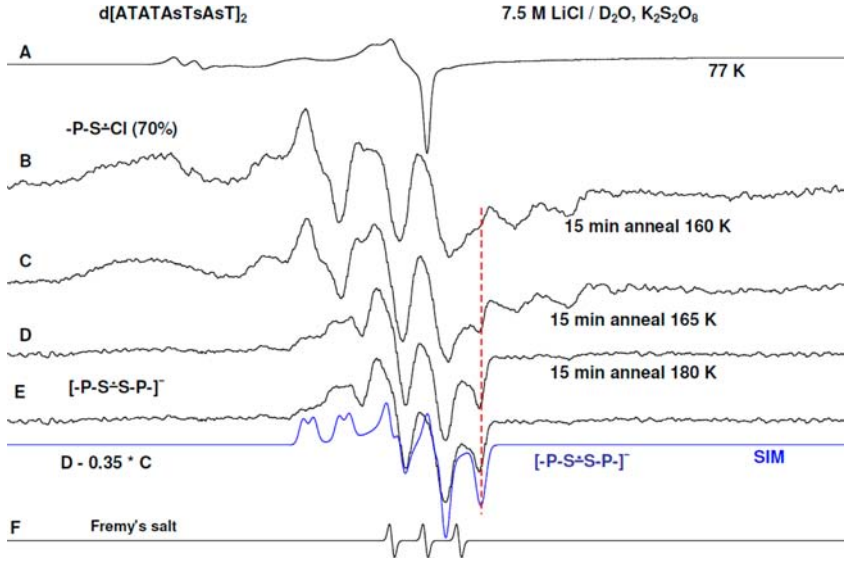


**Figure 2.** ESR spectra (black) of (A) $\gamma$-irradiated glassy sample of d[ATATAsTsAsT]$_2$ (1.5 mg/mL in 7.5 M LiCl/D$_2$O) in the presence of electron scavenger $K_2S_2O_8$ (9 mg/mL) at pH ~5. (B–D) Spectra found after annealing to (B) 160 K for 15 min, (C) 165 K for 15 min, and (D) 180 K for 15 min. (E) The black spectrum, obtained by subtracting 35% of spectrum (C) from spectrum (D), is the isolated spectrum of [-P-S∴S-P-]$^-$ in the ds S-oligomer. A line component from [-P-S∴S-P-]$^-$ that develops on annealing is indicated by the red dotted line. The blue spectrum in (E) is the simulated spectrum of [-P-S∴S-P-]$^-$. See text for details of simulation.

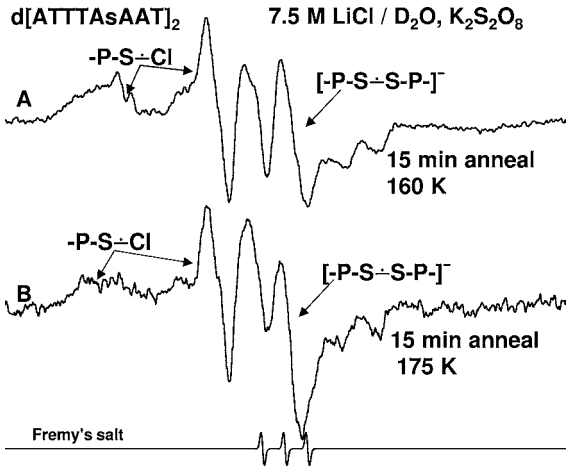


**Figure 3.** ESR spectra of (A) $\gamma$-irradiated (77 K) glassy sample of d[ATTTAsAAT]$_2$ (1.5 mg/mL in 7.5 M LiCl/D$_2$O) in the presence of electron scavenger $K_2S_2O_8$ (9 mg/mL) and found after annealing to 160 K for 15 min in the dark and (B) 175 K for 15 min.

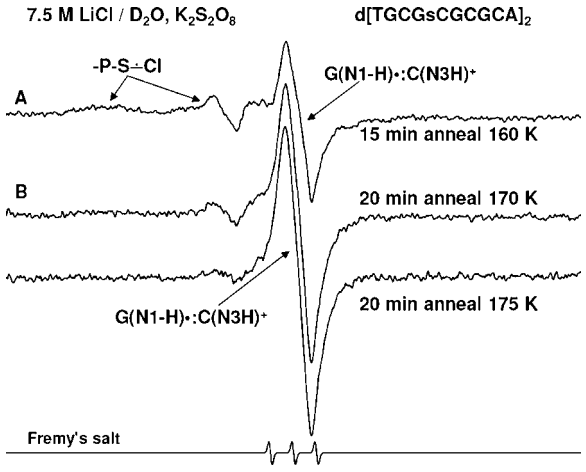


**Figure 4.** ESR spectra of (A) $\gamma$-irradiated (77 K) glassy sample of d[TGCGsCGCGCA]$_2$ (1.1 mg/mL in 7.5 M LiCl/D$_2$O) in the presence of electron scavenger $K_2S_2O_8$ (8 mg/mL) and found after annealing to 160 K for 15 min in the dark, (B) 170 K for 20 min, and (C) 175 K for 20 min.

Figure 4A. The ESR spectra found upon further annealing of this sample to 170 K and then to 175 K are shown in Figure 4B,C.

The spectrum in Figure 4A is composed of the -P-S∴Cl radical and a singlet spectrum. ESR characteristics of the singlet ($g$ value at the center, $g_\perp$, the total width, and the line shape which shows some poorly resolved hyperfine structure) match very well with the already published ESR spectrum of (G(N1-H)$^\bullet$:C(N3H)$^+$) found in ds oligomers[38,42,43] recorded under the same conditions (at 77 K at the native pD (~5) in 7.5 M LiCl/D$_2$O). Hence, the singlet found at the center of all spectra in Figure 4 is assigned to G(N1-H)$^\bullet$:C(N3H)$^+$ as the guanine moiety carries the hole (unpaired spin). The spectrum at 175 K shows that only the spectrum of G(N1-H)$^\bullet$:C(N3H)$^+$ is observed in a ds S-oligomer containing GC (Figure 4C). As a result, the bimolecular formation of [-P-S∴S-P-]$^-$ is not observed in d[TGCGsCGCGCA]$_2$ as found in d-[ATTTAsAAT]$_2$ samples (Figure 3).

The spectra in Figure 4 have been analyzed employing the black spectrum in Figure 1B as benchmark spectrum for -P-S∴Cl in a ds S-oligomer and the spectrum of G(N1-H)$^\bullet$:C(N3H)$^+$ from our previous work[38,42,43] as benchmark spectrum for G(N1-H)$^\bullet$:C(N3H)$^+$. These analyses confirm that the spectra in Figure 4A–C are due to two radicals, viz. -P-S∴Cl and G(N1-H)$^\bullet$:C(N3H)$^+$ .

Under the same conditions (constant gain and constant microwave power), the line components due to -P-S∴Cl progressively decrease on annealing (by a factor of ~4) while the singlet at the center due to G(N1-H)$^\bullet$:C(N3H)$^+$ increases by a factor of 2. This is a clear evidence for thermally activated hole transfer from -P-S∴Cl to G(N1-H)$^\bullet$:C(N3H)$^+$ which


dx.doi.org/10.1021/ja406121x | J. Am. Chem. Soc. 2013, 135, 12827–12838

occurs along with the usual radical−radical recombination that reduces the overall signal intensity. Thus, this work isolates the backbone-to-base hole-transfer pathway (Schemes 1 and 2). Our work shows that -P-S∴Cl results in one-electron oxidation of G only and not of A, C, or T. This brackets the redox potential of -P-S∴Cl between that of G (1.29 V) and that of A (1.42 V) at pH 7.[43,60]

*3.1.2.4. Electron Transfer from [-P-S-S-P-]$^-$ to G(N1-H)$^\bullet$:C(N3H)$^+$.* Employing d[TGCGsCsGCGCA]$_2$ as a model of a ds S-oligomer consisting of predominantly G and C but with two phosphorothioates, we investigate the competition of the formation of G(N1-H)$^\bullet$:C(N3H)$^+$ by thermally activated hole transfer from -P-S∴Cl (see Figure 4) with the unimolecular production of [-P-S∴S-P-]$^-$ (see Figure 2).

The ESR spectrum of a $\gamma$-irradiated sample of d-[TGCGsCsGCGCA]$_2$ at 77 K after annealing to 160 K for 15 min is shown in Figure 5A. In Figure 5B, the ESR spectrum (black) results from further annealing of this sample to 170 K.

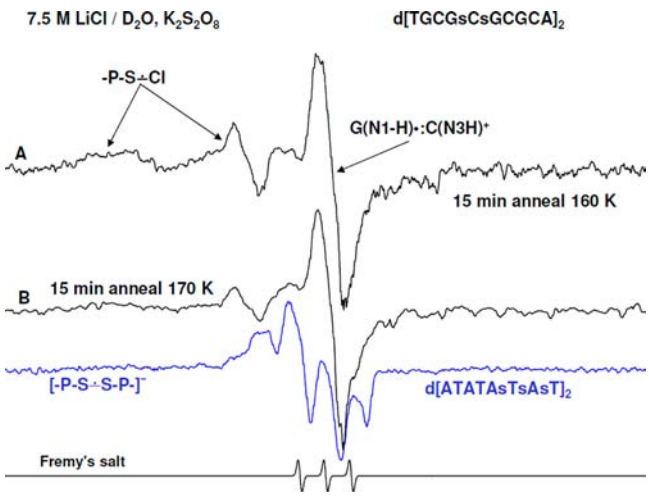


**Figure 5.** ESR spectra of (A) $\gamma$-irradiated (77 K) glassy sample of d[TGCGsCsGCGCA]$_2$ (1.6 mg/mL in 7.5 M LiCl/D$_2$O) in the presence of electron scavenger $K_2S_2O_8$ (9 mg/mL) and found after annealing to 160 K for 15 min in the dark and (B) 170 K for 15 min. The blue spectrum in (B) is the isolated spectrum of [-P-S∴S-P-]$^-$ in d[ATATAsTsAsT]$_2$ shown in Figure 2E.

The benchmark spectra -P-S∴Cl and G(N1-H)$^\bullet$:C(N3H)$^+$ used to analyze the spectra in Figure 4 have been employed in the analyses of spectra A and B in Figure 5.

Comparison of the spectrum in Figure 4A with that in Figure 5A shows that in d[TGCGsCGCGCA]$_2$ and in d-[TGCGsCsGCGCA]$_2$ samples, -P-S∴Cl formation dominates over the formation of one-electron-oxidized G (Scheme 2). From the ratio of -P-S∴Cl to G(N1-H)$^\bullet$:C(N3H)$^+$, the rate of reaction of $Cl_2^{\bullet-}$ with G appears to be about an order of magnitude lower that of $Cl_2^{\bullet-}$ with the >P═S moiety in the phosphorothioate group.

The analyses show that, on annealing, -P-S∴Cl decreases from 160 to 170 K, whereas G(N1-H)$^\bullet$:C(N3H)$^+$ also decreased slightly. The isolated spectrum (blue) of [-P-S∴S-P-]$^-$ in d[ATATAsTsAsT]$_2$ (already shown in Figure 2E) is shown under Figure 5B and makes up only a very small fraction of the overall signal of spectrum 5B (∼10−15%). Thus, the extent of formation of [-P-S∴S-P-]$^-$ is significantly lower than found for the AT S-oligomer in Figure 2. Moreover, the extent of formation of G(N1-H)$^\bullet$:C(N3H)$^+$ in Figure 5B is far less than found in Figure 4.

We find that a significant loss of the total radical signal from -P-S∴Cl, [-P-S∴S-P-]$^-$, and G(N1-H)$^\bullet$:C(N3H)$^+$ occurs on annealing from 160 to 170 K. This was not found in previous samples and suggests a reaction such as electron transfer from [-P-S∴S-P-]$^-$ to G(N1-H)$^\bullet$:C(N3H)$^+$, thereby leading to formation of neutral and diamagnetic [-P-S-S-P-] and GC (reaction 7):

As we observed in Figures 1−4, no observable line components due to sugar radicals are found in the spectra shown in Figure 5.

**3.2. Theoretical Results.** *3.2.1. Model Compound: Dimethyl Phosphorothioate.* Calculations using the B3LYP/6-31G* level of theory for dimethyl phosphorothioate (DMP) and diisopropyl phosphorothioate (DIP) show very similar results (see Supporting Information Table T1). The results for DMP are presented below for ease of description.

In order to test the extent of the decrease in ionization energy (IE) in phosphorothioate that would be expected due to substitution of the oxygen atom of the >P═O moiety in the sugar−phosphate backbone by a sulfur atom, DFT calculations have been performed employing the $\omega$B97x/6-31++G(d) method, which is known to provide accurate estimates of IE.[61] The gas-phase adiabatic ionization energies (AIEs) of DMP as a model system of the phosphorothioate backbone and AIE of dimethylphosphate as the model system of the phosphate backbone have been calculated. DMP has been charge neutralized by protonating the negatively charged oxygen atom, and this was compared to the corresponding analogous dimethyl phosphate also protonated at its negatively charged oxygen (see Supporting Information Figure S2). The zero-point-corrected (ZPC) AIE of phosphate backbone was calculated to be 10.02 eV, while the corresponding ZPC-AIE of phosphorothioate was calculated to be 8.71 eV. The lowering of the AIE in DMP by 1.29 eV is consistent with the decrease in IE expected from the literature, which shows that sulfur atom substitution for oxygen in a molecule lowers the IE by about 1.2−1.5 eV. For example, the experimentally determined IE of formaldehyde is 10.9 eV,[62] whereas that of $CH_2S$ is found to be 9.4 eV;[63] the IEs of ethanol (10.5 eV) vs ethanethiol (9.3 eV) and dimethyl ether (10.0 eV) vs dimethyl sulfide (8.7 eV) have been reported.[64] The 1.29 eV decrease in gas-phase AIE in the phosphorothioate places it in between those of the purines (G,A) and the pyrimidines (C,T).

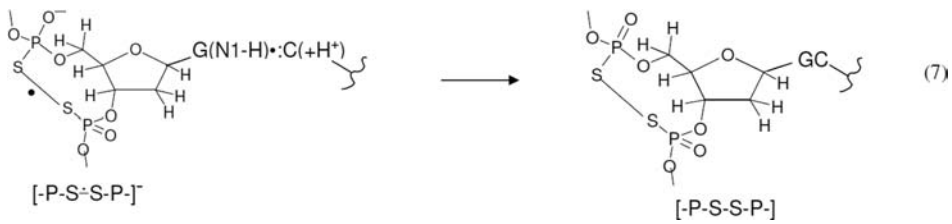


(7)


dx.doi.org/10.1021/ja406121x | J. Am. Chem. Soc. 2013, 135, 12827−12838

The bonding ($\sigma$) and antibonding ($\sigma^*$) molecular orbitals (MOs) for -P-S:Cl resulting from electrophilic addition of a Cl atom to the S in DMP, calculated using the B3LYP/6-31G* method, are shown in Figure 6. From Figure 6, it is evident

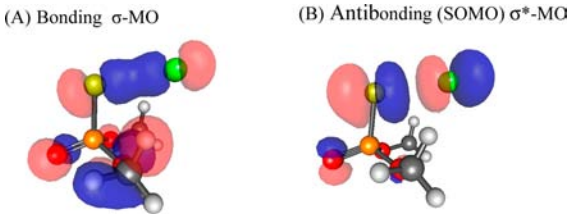


**Figure 6.** MOs for -P-S:Cl resulting from electrophilic Cl atom addition to sulfur on dimethyl phosphorothioate (DMP): (A) doubly occupied bonding $\sigma$-MO(38); (B) antibonding $\sigma^*$ singly occupied molecular orbital (SOMO) MO(46) calculated using the B3LYP/6-31G* optimized structure in the gas phase.

that, on the formation of the $\sigma^2\sigma^{*1}$ bond, the bonding $\sigma^2$ MO(38) stabilizes strongly and is located at 2.87 eV below the antibonding $\sigma^{*1}$ MO(46), which is designated as a singly occupied molecular orbital (SOMO).

The spin density distributions of -P-S:Cl and $[\text{-P-S:S-P-}]^-$ for DMP calculated at the B3LYP/6-31G* level in the gas phase are shown in Figure 7. In -P-S:Cl (Figure 7A), the unpaired

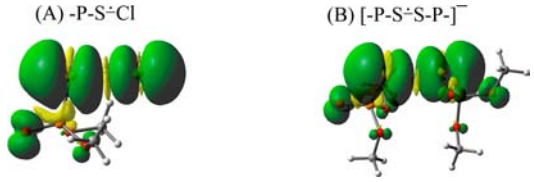


**Figure 7.** Spin density distributions in -P-S:Cl and $[\text{-P-S:S-P-}]^-$ of DMP employing the B3LYP/6-31G* method in the gas phase.

spin is localized to the antibonding $\sigma_p^*$ orbitals (see Figure 6B) on the S and Cl atoms. In $[\text{-P-S:S-P-}]^-$, the spin is localized on the two S−S atoms (Figure 7B), very similar to that obtained for -P-S:Cl.

The adiabatic electron affinity (AEA) and bond dissociation energy (BDE) of -P-S:Cl, $[\text{-P-S:S-P-}]^-$, and [-P-S-S-P-] for DMP, $[CH_3\text{-S:S-}CH_3]^-$, and $[CH_3\text{-S-S-}CH_3]$ have been calculated employing the B3LYP/6-31++G(d) method. These values are presented in Table 1 and have been compared with

**Table 1. B3LYP/6-31++G(d) Calculated Values of AEA and BDE of -P-S:Cl, $[\text{-P-S:S-P-}]^-$, and [-P-S-S-P-] for DMP, $[CH_3\text{-S:S-}CH_3]^-$, and $[CH_3\text{-S-S-}CH_3]$ in the Gas Phase**

| | | BDE, $D_e$ (kcal/mol) | |
|---|---|---|---|
| species | AEA (eV)[a] | this work | literature |
| -P-S:Cl | 2.75 | 37.2 | – |
| $[\text{-P-S:S-P-}]^-$ | – | 22.7 | – |
| [-P-S-S-P-] | 2.22 | 50.0 | – |
| $[CH_3\text{-S:S-}CH_3]^-$ | – | 24.7 | 26.8[b] |
| $[CH_3\text{-S-S-}CH_3]$ | 0.53[d] | 54.7 | 65.0[c] (61.8)[b] |

[a]AEA = $TE_{neutral} - TE_{anion}$ (TE = total energy). [b]Calculated using MP2/6-311+G (2d, 2p) method (see ref 65). [c]Experimentally determined value of $D_0$ (see ref 65). [d]Depending on the method, the calculated AEA of $[CH_3\text{-S-S-}CH_3]$ ranges from −0.09 to 0.35 eV (see ref 65).

those available in the literature.[65] These values lead to the following conclusions:

(i) The BDE value of $[\text{-P-S:S-P-}]^-$ for DMP is only slightly smaller than that of $[CH_3\text{-S:S-}CH_3]^-$. Also, [-P-S-S-P-] for DMP and $[CH_3\text{-S-S-}CH_3]$ have similar BDE values. As expected for addition of an antibonding electron to [-P-S-S-P-] and to $[CH_3\text{-S-S-}CH_3]$ forming $[\text{-P-S:S-P-}]^-$ and $[CH_3\text{-S:S-}CH_3]^-$, the bond strength decreases almost by a factor of 2 and the S−S bond lengths of the optimized structures of anion radicals increase (2.83, 2.87 Å) over the diamagnetic neutral species (2.10, 2.10 Å).

(ii) The gas-phase AEA values of [-P-S-S-P-] and $[CH_3\text{-S-S-}CH_3]$ (Table 1) are in accord with their reduction potential values (see Table 3, below) calculated using the B3LYP/6-31++G(d) method.

The experimentally obtained $A_{\|}$ HFCC value for $^{35}$Cl in -P-S:Cl from DIP is 67 G (Table 2). From this value and the value of 204 G is that expected for a full spin on Cl[58] an estimate of the spin density on the Cl atom in -P-S:Cl can be calculated as (67 G/204 G) = 0.33. The theoretically calculated spin density values of S and Cl atoms of -P-S:Cl from DMP are obtained as 0.55 and 0.40, respectively. Thus, the experimentally found spin density value of Cl atom in -P-S:Cl for DIP is a reasonable match with that found for DMP obtained by theory. As found by experiment and theory, the predominant spin density is on the S atom in -P-S:Cl.

The theoretically calculated anisotropic components of HFCC values of the $\alpha$ P atom in -P-S:Cl of DMP are found to be very small which predict that the $\alpha$ P atom in -P-S:Cl should have a near isotropic hyperfine coupling. This is supported by experiment (see Figure 1 and Table 2). However, the theoretically calculated HFCC value of the $\alpha$ P atom in -P-S:Cl is found to be ∼10 G smaller than that of its experimentally obtained value (Table 2) and this is a common issue with DFT calculations of phosphorus couplings.[66] We note here that the good agreements of the spin density value and HFCC value of the $\alpha$ Cl atom of -P-S:Cl supports our assignment of the spectra in Figure 1B to -P-S:Cl.

The spin density distribution calculated employing the B3LYP/6-31G* DFT method for $[\text{-P-S:S-P-}]^-$ in DMP (Figure 7B) shows an equal distribution of spins on both S atoms as expected. Calculations also predict roughly equal distribution of spins on both $\alpha$ P atoms (Figure 7B); hence, the HFCC values of these $\alpha$ P atoms are found to have a small difference (∼2 G) from each other (Table 2). Theoretically calculated anisotropic components of HFCC values of both $\alpha$ P atoms in $[\text{-P-S:S-P-}]^-$ are found to be very small (Table 2). Thus, calculations suggest that both $\alpha$ P atoms in $[\text{-P-S:S-P-}]^-$ have nearly isotropic hyperfine coupling. This lack of anisotropy in the $\alpha$ P atom HFCCs is also found in our experimental results (section 3.1). However, the experimentally obtained HFCC values of $\alpha$ P atoms in $[\text{-P-S:S-P-}]^-$ substantially differ, with couplings of ∼16 and ∼7.5 G. Moreover, the theoretically calculated maximum HFCC value of the $\alpha$ P atom ($P_2$) in $[\text{-P-S:S-P-}]^-$ is found to be ∼4−5 G smaller than the experimentally obtained value (Table 2). Again, this underestimation of P atom HFCC values by DFT is expected from the literature.[66]

*3.2.2. Model S-Oligomer (AsAs).* Because the B3LYP method was found to be unsuitable for stacked systems,[53] the M06-2x/6-31G** method was employed to find the optimized structure (Figure 8B) of $[\text{-P-S:S-P-}]^-$ in AsAs. Thereafter, the


dx.doi.org/10.1021/ja406121x | J. Am. Chem. Soc. 2013, 135, 12827−12838

**Table 2. HFCC Values (in Gauss) Obtained by Theory and Experiment; B3LYP/6-31G* Method Has Been Used for the Calculation**

| | | | HFCC (G) | | | |
|---|---|---|---|---|---|---|
| | | | theory | | | |
| molecule | radical | atom | $A_{Iso}$ | $A_{Aniso}$ | total | exp[a] |
| DMP | -P-S-Cl | P | −12.31 | −0.47 | −12.78 | ∼23 |
| | | | | 0.05 | −12.26 | |
| | | | | 0.42 | −11.89 | |
| | | $^{35}$Cl | 22.41 | −24.25 | −1.84 | 0 |
| | | | | −24.20 | −1.79 | 0 |
| | | | | 48.46 | 70.87 | 67[b] |
| | [-P-S-S-P-]$^-$ | P1 | −8.92 | −0.88 | −9.80 | (6.0, 9.0, 7.0) |
| | | | | −0.27 | −9.19 | |
| | | | | 1.15 | −7.77 | |
| | | P2 | −11.33 | −0.56 | −11.89 | (16.0, 16.0, 17.0) |
| | | | | −0.22 | −11.56 | |
| | | | | 0.77 | −10.56 | |
| AsAs[c] | [-P-S-S-P-]$^-$ | P1 | −0.14 | −1.87 | −2.01 | (2.0, 4.0, 4.0) |
| | | | | −1.09 | −1.23 | |
| | | | | 2.96 | 2.82 | |
| | | P2 | −13.47 | −0.90 | −14.37 | (14.0, 16.0, 14.0) |
| | | | | −0.25 | −13.72 | |
| | | | | 1.15 | −12.32 | |

[a]Experiment gives the magnitude but not the sign of the coupling. [b]The $^{35}$Cl isotope has 75% abundance. [c]Geometry was fully optimized using the M06-2x/6-31G** method.

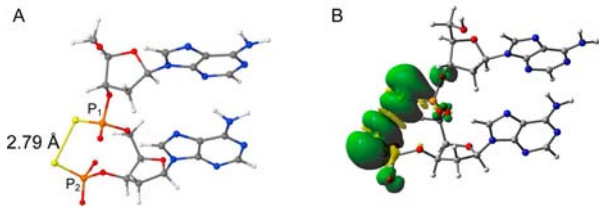


**Figure 8.** (A) M06-2x/6-31G** fully optimized structure of [-P-S-S-P]$^-$ in AsAs in the gas phase. The two $\alpha$ P atoms are indicated by $P_1$ and $P_2$. (B) Spin density distribution for the structure in (A).

B3LYP/6-31G* method was employed to calculate the spin density distributions (Figure 8A) and HFCC values in [-P-S-S-P-]$^-$ in AsAs using the M06-2x/6-31G**-optimized geometries. Comparison of the spin density distribution of [-P-S-S-P-]$^-$ in DMP (Figure 7B) with that of [-P-S-S-P-]$^-$ in AsAs (Figure 8A) shows that the S atoms in both radicals have almost equal spin densities.

The B3LYP/6-31G*-calculated HFCC values of [-P-S-S-P-]$^-$ in AsAs are shown in Table 2. For DMP, where the theoretically predicted HFCC values of two $\alpha$ P atoms are almost equal (Figure 6B, Table 2), the theoretically calculated HFCC values of the two $\alpha$ P atoms of [-P-S-S-P-]$^-$ for AsAs are not equal—a dominant $\alpha$ P atom HFCC (shown as P2 in Figure 8B) and a much smaller $\alpha$ P atom HFCC (shown as P1 in Figure 8B). In Table 2, we present a comparison of the calculated and experimentally obtained HFCC values of these two $\alpha$ P atoms of [-P-S-S-P-]$^-$ for AsAs. There is a good agreement between the calculated and experimental HFCC values of [-P-S-S-P-]$^-$ for AsAs, in contrast to DMP or DIP, where the theoretically calculated HFCC values of [-P-S-S-P-]$^-$ are found to be larger than those obtained by experiments.

*3.2.3. Calculated Values of Reduction Potentials of [$CH_3$-P-S-S-P-$CH_3$]$^-$, [$CH_3$-S-S-$CH_3$]$^-$, and $O_2$.* Estimates of the reduction potentials of the various [-P-S-S-P-]$^-$ radicals studied in this work are of interest, as these species result from the one-electron oxidation of vicinal phosphorothioates in S-oligomers. Thus, the reduction potential of [$CH_3$-P-S-S-P-$CH_3$]$^-$ has been calculated and compared to two other species. We have found in this work that, in contrast to disulfide anion radicals [R-S-S-R]$^-$,[59] [-P-S-S-P-]$^-$ does not cause one-electron reduction of $O_2$. Therefore, the reduction potentials of [$CH_3$-S-S-$CH_3$]$^-$ and $O_2$ have also been calculated. The $\omega$B97x/6-31++G(d) method is employed for these calculations, as it has provided quite accurate values of ionization potentials of the DNA bases.[61] We note here that the reduction potentials of these three species have been calculated employing the B3LYP/6-31++G(d) method as well for comparison. These results are presented in Table 3.

The experimental reduction potential for $O_2$ is known (Table 3). Although the value of the reduction potential of [$CH_3$-S-S-$CH_3$]$^-$ is not available in the literature, corresponding values for similar structures, cystine and glutathione

**Table 3. Calculated Reduction Potentials of [$CH_3$-P-S-S-P-$CH_3$], [$CH_3$-S-S-$CH_3$], and $O_2$**

| | $E°$ (V) | |
|---|---|---|
| redox couple | theory[a] | experiment |
| [$CH_3$-P-S-S-P-$CH_3$]/[$CH_3$-P-S-S-P-$CH_3$]$^-$ | −0.31 (−0.25) | – |
| [$CH_3$-S-S-$CH_3$]/[$CH_3$-S-S-$CH_3$]$^-$ | −1.95 (−1.68) | −1.5 (cystine)[67] |
| | | −1.47 (dithiothreitol)[68] |
| $O_2$/$O_2^{\bullet-}$ | −0.53 (−0.39) | −0.33[67] |

[a]Reduction potentials calculated using the $\omega$B97x/6-31++G(d) and B3LYP/6-31++G(d) methods incorporating the SMD model for solvation. Calculated potentials are in reference to $E°$ ($H^+/H_2$) = 4.44 V (see ref 70). B3LYP results are presented in parentheses.


dx.doi.org/10.1021/ja406121x | J. Am. Chem. Soc. 2013, 135, 12827−12838

disulfide anion radicals (−1.5 V)[67] as well as another disulfide anion radical from dithiothreitol, −1.47 V,[68] have been reported.

The calculated results in Table 3 clearly predict that $[CH_3\text{-}S\therefore S\text{-}CH_3]^-$ is much more reducing than $O_2^{\bullet-}$, while $O_2^{\bullet-}$ is somewhat more reducing than $[CH_3\text{-}P\text{-}S\therefore S\text{-}P\text{-}CH_3]^-$ (see Table 1 for AEA values). Hence, the calculated reduction potentials indicate that [-P-S∴S-P-]$^-$ should not undergo electron transfer to $O_2$ as found in this work (Figure 5); however, as predicted, R-S∴S-R$^-$ does transfer its excess electron to $O_2$, which is well-established in previous works.[59] Experiment shows that the reduction potential of [-P-S∴S-P-]$^-$ must be higher than that of $O_2$ (−0.33 V[67]). The calculated reduction potential values −0.53(−0.39) V for $O_2$ vs −0.31(−0.25) V for $[CH_3\text{-}P\text{-}S\therefore S\text{-}P\text{-}CH_3]^-$ support this experimental observation.

## 4. CONCLUSIONS

The present work on one-electron oxidation reactions of phosphorothioate groups in S-oligmers and model compounds leads to the following salient points.

**4.1. Formation of $\sigma^2\sigma^{*1}$-Bonded -P-S∴Cl.** ESR and theoretical studies presented in this work provide clear evidence of electrophilic reaction of $Cl_2^{\bullet-}$ with phosphorothioates (DIP and ds S-oligomers), producing the chlorine atom adduct, -P-S∴Cl, with the elimination of Cl$^-$ (reaction 4 and Scheme 2). The spin density distributions of the S and Cl atoms in -P-S∴Cl and the molecular orbital nature for the $\sigma^2$ bonding MO and the $\sigma^{*1}$ antibonding SOMO are as expected for the formation of a two-center three-electron $\sigma^2\sigma^{*1}$-bond between the S and Cl atoms in -P-S∴Cl.

As expected, ESR spectra of P-S-Cl in both DIP and AT S-oligomers clearly show the line components of $^{35}$Cl and $^{37}$Cl isotopes of Cl along with a single $\alpha$ P atom isotropic hyperfine coupling. Experimental HFCC values of Cl and of P and spin density calculations show that the unpaired spin is mainly (∼67%) located on the S atom of -P-S∴Cl.

**4.2. Formation of $\sigma^2\sigma^{*1}$-Bonded [-P-S∴S-P-]$^-$ in DIP and in ds S-Oligomers.** For the small molecular species DIP, we find complete bimolecular formation of $\sigma^2\sigma^{*1}$-bonded [-P-S∴S-P-]$^-$ via reaction 5 upon annealing to 165 K. For the far larger ds S-oligomers, the reaction to disulfide anion radicals is incomplete and varies in extent with the nature of the S-oligomer. In ds S-oligomers of AT with multiple phosphorothioates at close proximity, substantial but not complete unimolecular formation of only [-P-S∴S-P-]$^-$ has been observed (Scheme 3) via annealing to 175−180 K. On the other hand, for ds S-oligomers of AT with one phosphorothioate on each strand, a lower extent of [-P-S∴S-P-]$^-$ formation, likely from inter-strand reaction, is found. Clearly, the rate and extent of formation of [-P-S∴S-P-]$^-$ are governed by the number and proximity of phosphorothioates within the DNA structure (Scheme 3).

**4.3. Backbone-to-Base Hole-Transfer Process Found in ds S-Oligomers with G.** Annealing of samples of ds S-oligomers containing one or more G in the range 160−175 K results in the one-electron oxidation of G, forming G(N1-H)$^\bullet$:C(N3H)$^+$ via thermally activated hole transfer from -P-S∴Cl. This is direct evidence of a backbone-to-base hole-transfer process. Furthermore, -P-S∴Cl induces one-electron oxidation of G only and not of A, C, or T. Thus, the redox potential of -P-S∴Cl is higher than that of G but lower than those of A, C, and T. The reported redox potentials of G, A, C, and T[60] bracket the redox potential of -P-S∴Cl between the redox potentials of G and A, i.e., between 1.29 and 1.42 V. This is a relatively small range and gives a good estimate of the redox potential for -P-S∴Cl as 1.35 ± 0.07 V.

**4.4. [-P-S∴S-P-]$^-$ Does Not Undergo an Electron-Transfer Reaction with $O_2$.** Our ESR studies as well as the calculated values of AEA and reduction potentials in this work clearly point out that, unlike the disulfide anion radicals [R-S∴S-R]$^-$ such as cystine, the glutathione disulfide anion radical[59,68] [-P-S∴S-P-]$^-$ does not undergo an electron-transfer reaction to $O_2$. Further, ESR studies show that formation of -P-S∴Cl is not affected by the presence of oxygen. Oxygen would therefore not affect the backbone-to-base hole-transfer process in ds S-oligomers.

**4.5. Electron Transfer from [-P-S∴S-P-]$^-$ to G(N1-H)$^\bullet$:C(N3H)$^+$ in ds S-Oligomers.** Our ESR studies in ds S-oligomers containing G with more than one phosphorothioate group present clear evidence of electron transfer from [-P-S∴S-P-]$^-$ to G(N1-H)$^\bullet$:C(N3H)$^+$. Since [-P-S∴S-P-]$^-$ does not undergo electron-transfer reaction with molecular oxygen, G(N1-H)$^\bullet$:C(N3H)$^+$ is chemically repaired back to the GC pair, even in the presence of oxygen. Thus, in these ds S-oligomers, the subsequent reactions of G(N1-H)$^\bullet$:C(N3H)$^+$ to form molecular products, such as 8-hydroxy-7,8-dihydroguanine and 2,6-diamino-4-hydroxy-5-formamidopyrimidine,[4,45,69] would be prevented at the expense of formation of the neutral diamagnetic product [-P-S-S-P-] (reaction 7 and Scheme 3).

The phosphorothioate disulfide link, [-P-S-S-P-], is predicted to have a stable disulfide bond of 50 kcal/mol and thus, once formed in the DNA backbone, would be a significant impediment to DNA replication or transcription.

## ■ ASSOCIATED CONTENT

### Ⓢ Supporting Information

Comparison of the theoretically calculated HFCC values of the radicals found in DMP and in DIP (Table T1); formation of [-P-S∴S-P-]$^-$ from -P-S∴Cl in the AT mismatch in the S-oligomer d[ATATAsAsAsT]$_2$ (Figure S1); fully optimized structures ($\omega$B97x/6-31++G(d)) of neutral parent molecule and cation radical of protonated dimethyl phosphate and of protonated DMP in the gas phase. This material is available free of charge via the Internet at http://pubs.acs.org.

## ■ AUTHOR INFORMATION

### Corresponding Author

sevilla@oakland.edu.

### Notes

The authors declare no competing financial interest.

## ■ ACKNOWLEDGMENTS

We thank the National Cancer Institute of the National Institutes of Health (Grant RO1CA045424) for support.

## ■ REFERENCES

(1) Ward, J. F. *Cold Spring Harb. Symp. Quant. Biol.* **2000**, *65*, 377−382.

(2) Kanaar, R.; Hoeijmakers, J. H.; van Gent, D. C. *Trends Cell Biol.* **1998**, *8*, 483−489.

(3) Frankenberg, D.; Frankenberg-Schwager, M.; Blöcher, D.; Harbich, R. *Radiat. Res.* **1981**, *88*, 524−532.

(4) von Sonntag, C. *Free-Radical-Induced DNA Damage and Its Repair*; Springer-Verlag: Heidelberg, 2006.

(5) Becker, D.; Adhikary, A.; Sevilla, M. D. In *Charge Migration in DNA: Physics, Chemistry and Biology Perspectives*; Chakraborty, T., Ed.; Springer-Verlag: Berlin/Heidelberg/New York, 2007; pp 139−175.
(6) Becker, D.; Adhikary, A.; Sevilla, M. D. In *Recent Trends in Radiation Chemistry*; Rao, B. S. M., Wishart, J., Eds.; World Scientific Publishing Co.: Singapore/New Jersey/London, 2010; pp 509−542.
(7) Becker, D.; Adhikary, A.; Sevilla, M. D. In *Charged Particle and Photon Interactions with Matter—Recent Advances, Applications, and Interfaces*; Hatano, Y., Katsumura, Y., Mozumder, A., Eds.; CRC Press/Taylor & Francis Group: Boca Raton/London/New York, 2010; pp 503−541.
(8) Pogozelski, W. K.; Tullius, T. D. *Chem. Rev.* **1998**, *98*, 1089−1108.
(9) Greenberg, M. M. *Org. Biomol. Chem.* **2007**, *5*, 18−30.
(10) Dedon, P. C. *Chem. Res. Toxicol.* **2008**, *21*, 206−219.
(11) Bernhard, W. A. In *Radical and Radical Ion Reactivity in Nucleic Acid Chemistry*; Greenberg, M. M., Ed.; John Wiley & Sons, Inc.: Hoboken, NJ, 2009; pp 41−68.
(12) Close, D. M. In *Radiation-induced Molecular Phenomena in Nucleic Acids: A Comprehensive Theoretical and Experimental Analysis*; Shukla, M. K., Leszczynski, J., Eds.; Springer-Verlag: Berlin/Heidelberg/New York, 2008; pp 493−529.
(13) Chatgilialoglu, C. In *Radical and Radical Ion Reactivity in Nucleic Acid Chemistry*; Greenberg, M. M., Ed.; John Wiley & Sons, Inc.: Hoboken, NJ, 2009; pp 99−133.
(14) Adhikary, A.; Becker, D.; Palmer, B. J.; Heizer, A. N.; Sevilla, M. D. *J. Phys. Chem. B* **2012**, *116*, 5900−5906.
(15) Close, D. M. *Radiat. Res.* **1997**, *147*, 663−673.
(16) Kumar, A.; Sevilla, M. D. *J. Phys. Chem. B* **2009**, *113*, 13374−13380.
(17) Khanduri, D.; Collins, S.; Kumar, A.; Adhikary, A.; Sevilla, M. D. *J. Phys. Chem. B* **2008**, *112*, 2168−2178.
(18) Adhikary, A.; Khanduri, D.; Kumar, A.; Sevilla, M. D. *J. Phys. Chem. B* **2008**, *112*, 15844−15855.
(19) Kumar, A.; Sevilla, M. D. *J. Phys. Chem. B* **2006**, *110*, 24181−24188.
(20) Swarts, S. G.; Sevilla, M. D.; Becker, D.; Tokar, C. J.; Wheeler, K. T. *Radiat. Res.* **1992**, *129*, 333−344.
(21) Swarts, S. G.; Becker, D.; Sevilla, M. D.; Wheeler, K. T. *Radiat. Res.* **1996**, *145*, 304−314.
(22) Becker, D.; Adhikary, A.; Tetteh, S. T.; Bull, A. W.; Sevilla, M. D. *Radiat. Res.* **2012**, *178*, 524−537.
(23) Eckstein, F. *Antisense Nucleic Acid Drug Dev.* **2000**, *10*, 117−121.
(24) Dias, N.; Stein, C. A. *Mol. Cancer Ther.* **2002**, *1*, 347−355.
(25) Chan, J. H. P.; Lim, S.; Wong, W. S. F. *Clin. Exp. Pharmacol. Physiol.* **2006**, *33*, 533−540.
(26) Wang, L.; Chen, S.; Xu, T.; Taghizadeh, K.; Wishnok, J. S.; Zhou, X.; You, D.; Deng, Z.; Dedon, P. C. *Nat. Chem. Biol.* **2007**, *11*, 709−710.
(27) Cruse, W. B. T.; Salisbury, S. A.; Brown, T.; Cosstick, R.; Eckstein, F.; Kennard, O. *J. Mol. Biol.* **1986**, *192*, 891−905.
(28) Ozaki, H.; McLaughlin, L. W. *Nucleic Acids Res.* **1992**, *20*, 5205−5214.
(29) Black, P. J.; Bernhard, W. A. *J. Phys. Chem. B* **2011**, *115*, 8009−8013.
(30) Adhikary, A.; Kumar, A.; Becker, D.; Sevilla, M. D. In *Encyclopedia of Radicals in Chemistry, Biology and Materials*; Chatgilialoglu, C., Struder, A., Eds.; John Wiley & Sons Ltd.: Chichester, UK, 2012; pp 1371−1396.
(31) Adhikary, A.; Malkhasian, A. Y. S.; Collins, S.; Koppen, J.; Becker, D.; Sevilla, M. D. *Nucleic Acids Res.* **2005**, *33*, 5553−5564.
(32) Adhikary, A.; Becker, D.; Collins, S.; Koppen, J.; Sevilla, M. D. *Nucleic Acids Res.* **2006**, *34*, 1501−1511.
(33) Adhikary, A.; Kumar, A.; Becker, D.; Sevilla, M. D. *J. Phys. Chem. B* **2006**, *110*, 24171−24180.
(34) Adhikary, A.; Khanduri, D.; Kumar, A.; Sevilla, M. D. *J. Phys. Chem. B* **2008**, *112*, 15844−15855.
(35) Becker, D.; Adhikary, A.; Khanduri, D.; Sevilla, M. D. *AIP Conf. Proc.* **2009**, *1197*, 201−208.
(36) Adhikary, A.; Khanduri, D.; Pottiboyina, V.; Rice, C. T.; Sevilla, M. D. *J. Phys. Chem. B* **2010**, *114*, 9289−9299.
(37) Adhikary, A.; Kumar, A.; Heizer, A. N.; Palmer, B. J.; Pottiboyina, V.; Liang, Y.; Wnuk, S. F.; Sevilla, M. D. *J. Am. Chem. Soc.* **2013**, *135*, 3121−3135.
(38) (a) Adhikary, A.; Khanduri, D.; Sevilla, M. D. *J. Am. Chem. Soc.* **2009**, *131*, 8614−8619. (b) Adhikary, A.; Sevilla, M. D. *J. Phys. Chem. B* **2011**, *115*, 8947−8948.
(39) Adhikary, A.; Kumar, A.; Khanduri, D.; Sevilla, M. D. *J. Am. Chem. Soc.* **2008**, *130*, 10282−10292.
(40) Adhikary, A.; Kumar, A.; Sevilla, M. D. *Radiat. Res.* **2006**, *165*, 479−484.
(41) Adhikary, A.; Collins, S.; Khanduri, D.; Sevilla, M. D. *J. Phys. Chem. B* **2007**, *111*, 7415−7421.
(42) Adhikary, A.; Kumar, A.; Munafo, S. A.; Khanduri, D.; Sevilla, M. D. *Phys. Chem. Chem. Phys.* **2010**, *12*, 5353−5368.
(43) Khanduri, D.; Adhikary, A.; Sevilla, M. D. *J. Am. Chem. Soc.* **2011**, *133*, 4527−4537.
(44) O'Neill, M.; Barton, J. K. *J. Am. Chem. Soc.* **2004**, *126*, 13234−13235.
(45) (a) Shukla, L. I.; Adhikary, A.; Pazdro, R.; Becker, D.; Sevilla, M. D. *Nucleic Acids Res.* **2004**, *32*, 6565−6574. (b) Shukla, L. I.; Adhikary, A.; Pazdro, R.; Becker, D.; Sevilla, M. D. *Nucleic Acids Res.* **2007**, *35*, 2460−2461.
(46) Becke, A. D. *J. Chem. Phys.* **1993**, *98*, 1372−1377.
(47) Stephens, P. J.; Devlin, F. J.; Frisch, M. J.; Chabalowski, C. F. *J. Phys. Chem.* **1994**, *98*, 11623−11627.
(48) Lee, C.; Yang, W.; Parr, R. G. *Phys. Rev. B* **1988**, *37*, 785−789.
(49) Hermosilla, L.; Calle, P.; García de la Vega, J. M.; Sieiro, C. *J. Phys. Chem. A* **2005**, *109*, 1114−1124.
(50) Hermosilla, L.; Calle, P.; García de la Vega, J. M.; Sieiro, C. *J. Phys. Chem. A* **2006**, *110*, 13600−13608.
(51) Barone, V.; Cimino, P. *Chem. Phys. Lett.* **2008**, *454*, 139−143.
(52) Close, D. M. *J. Phys. Chem. A* **2010**, *114*, 1860−1187.
(53) Zhao, Y.; Truhlar, D. G. *Theor. Chem. Acc.* **2008**, *120*, 215−241.
(54) Frisch, M. J.; Trucks, G. W.; Schlegel, H. B.; Scuseria, G. E.; Robb, M. A.; Cheeseman, J. R.; Scalmani, G.; Barone, V.; Mennucci, B.; Petersson, G. A.; Nakatsuji, H.; Caricato, M.; Li, X.; Hratchian, H. P.; Izmaylov, A. F.; Bloino, J.; Zheng, G.; Sonnenberg, J. L.; Hada, M.; Ehara, M.; Toyota, K.; Fukuda, R.; Hasegawa, J.; Ishida, M.; Nakajima, T.; Honda, Y.; Kitao, O.; Nakai, H.; Vreven, T.; Montgomery, J. A., Jr.; Peralta, J. E.; Ogliaro, F.; Bearpark, M.; Heyd, J. J.; Brothers, E.; Kudin, K. N.; Staroverov, V. N.; Kobayashi, R.; Normand, J.; Raghavachari, K.; Rendell, A.; Burant, J. C.; Iyengar, S. S.; Tomasi, J.; Cossi, M.; Rega, N.; Millam, J. M.; Klene, M.; Knox, J. E.; Cross, J. B.; Bakken, V.; Adamo, C.; Jaramillo, J.; Gomperts, R.; Stratmann, R. E.; Yazyev, O.; Austin, A. J.; Cammi, R.; Pomelli, C.; Ochterski, J. W.; Martin, R. L.; Morokuma, K.; Zakrzewski, V. G.; Voth, G. A.; Salvador, P.; Dannenberg, J. J.; Dapprich, S.; Daniels, A. D.; Farkas, O.; Foresman, J. B.; Ortiz, J. V.; Cioslowski, J.; Fox, D. J. *Gaussian 09*; Gaussian, Inc.: Wallingford, CT, 2009.
(55) *GaussView*; Gaussian, Inc.: Pittsburgh, PA, 2003.
(56) *IQmol*, Free open-source molecular editor and visualization package; available at http://www.iqmol.org.
(57) Yu, X.-Y.; Bao, Z.-C.; Barker, J. R. *J. Phys. Chem. A* **2004**, *108*, 295−308.
(58) Champagne, M. H.; Mullins, M. W.; Colson, A.-O.; Sevilla, M. D. *J. Phys. Chem.* **1991**, *95*, 6487−6493.
(59) von Sonntag, C. *The Chemical Basis of Radiation Biology*; Taylor & Francis: London/New York, 1987; p 366 and references therein.
(60) The reduction potential at pH 7 (i.e., midpoint potential ($E_7$)) values of the DNA components at room temperature in aqueous solutions are $E_7$(dG(-H)$^{\bullet}$/dG) = 1.29 V, $E_7$(dA(-H)$^{\bullet}$/dA) = 1.42 V, $E_7$(dT$^{\bullet}$/dT) = 1.7 V, $E_7$(dC$^{\bullet}$/dC) = 1.6 V, and $E_7$ (dR$^{\bullet}$/dR) ≫ 1.8 V (dR = 2′-deoxyribose). The p$K_a$ of the guanine cation radical (G$^{\bullet+}$) being 3.9, the reduction potential of G$^{\bullet+}$ is reported as $E^{\circ}$ = 1.58 V. See: Steenken, S.; Jovanovic, S. V. *J. Am. Chem. Soc.* **1997**, *119*, 617−618 and ref 43.

(61) Kumar, A.; Pottiboyina, V.; Sevilla, M. D. *J. Phys. Chem. B* **2012**, *116*, 9409−9416.
(62) NIST website: http://cccbdb.nist.gov/ie2.asp?casno=50000.
(63) Ruscic, B.; Berkowitz, J. *J. Chem. Phys.* **1993**, *98*, 2568−2579.
(64) NIST Chemistry Webbook. http://webbook.nist.gov/, 2002.
(65) Carles, S.; Lecomte, F.; Schermann, J. P.; Desfrancüois, C.; Xu, S.; Nilles, J. M.; Bowen, K.; Bergès, J.; Houée-Levin, C. *J. Phys. Chem. A* **2001**, *105*, 5622−5626.
(66) Nguyen, M. T.; Creve, S.; Vanquickenborne, L. G. *J. Phys. Chem. A* **1997**, *101*, 3174−3181.
(67) Buettner, G. R. *Arch. Biochem. Biophys.* **1993**, *300*, 535−543.
(68) Surdhar, P. S.; Armstrong, D. A. *J. Phys. Chem.* **1987**, *91*, 6532−6537.
(69) Cadet, J.; Douki, T.; Gasparutto, D.; Ravanat, J.-L.; Wagner, J. R. In *Radical and Radical Ion Reactivity in Nucleic Acid Chemistry*; Greenberg, M. M., Ed.; John Wiley & Sons, Inc.: Hoboken, NJ, 2009; pp 69−99.
(70) Trasatti, S. *Pure Appl. Chem.* **1986**, *58*, 955−966.